



1 **A fracture mechanics framework for optimising design and**
2 **inspection of offshore Wind Turbine support structures against**
3 **fatigue failure**
4

5 Peyman Amirafshari¹, Feargal Brennan¹, Athanasios Kolios¹

6 ¹Department of Naval Architecture, Ocean and Marine Engineering, University of Strathclyde,
7 Glasgow, G4 0LZ, United Kingdom

8 *Correspondence to:* Peyman Amirafshari (amirafshari.peyman@strath.ac.uk)

9 **Abstract**

10 Offshore Wind Turbine (OWT) support structures need to be designed against fatigue failure
11 under cyclic aerodynamic and wave loading. The fatigue failure can be accelerated in a corrosive
12 sea environment. Traditionally, a stress-life approach called the S-N curve method has been
13 used for design of structures against fatigue failure. There are a number of limitations in S-N
14 approach related to welded structures which can be addressed by the fracture mechanics
15 approach. In this paper the limitations of the S-N approach related to OWT support structure
16 are addressed, a fatigue design framework based on fracture mechanics is developed. The
17 application of the framework to a monopile OWT support structure is demonstrated and
18 optimisation of in-service inspection of the structure is studied. It was found that both the design
19 of the weld joint and Non-destructive testing techniques can be optimised to reduce In-service
20 frequency. Furthermore, probabilistic fracture mechanics as a form of risk-based design is
21 outlined and its application to the monopile support structure is studied. The probabilistic model
22 showed to possess a better capability to account for NDT reliability over a range of possible
23 crack sizes as well as providing a risk associated with the chosen inspection time which can be
24 used in inspection cost benefit analysis. There are a number of areas for future research.
25 including better estimate of fatigue stress with a time-history analysis, the application of
26 framework to other types of support structures such as Jackets and Tripods, and integration of
27 risk-based optimisation with a cost benefit analysis.

28 **1 Introduction**

29 Wind turbines are playing a key role in decarbonising world power production system. Target
30 share of energy from renewable sources in European Union (EU) countries set out by National
31 Energy and Climate Plans (NECPs) is aimed to reach 32% by 2030 and 100% by 2050. In 2018
32 the total share of energy from renewable sources were 18% in EU and 16% in United Kingdom
33 (European Environment Agency, 2019). Thanks to commitment of European countries to
34 achieve the above targets the prospects for the offshore renewable industry for further growth
35 continues to be strong (Fraile et al., 2019).

36 Since the power production of a wind turbine is directly related to the wind velocity at the hub,
37 the developments of Offshore Wind Turbine (OWT) are expected to grow in order to harvest
38 more power from offshore sites where wind speed is generally higher compared to the onshore.

39 Despite their higher wind power capacity, the biggest disadvantage of OWTs is their
40 construction and maintenance costs. Due to their remote location their inspection and
41 maintenance is challenging and expensive. Therefore, optimising design and maintenance of



42 these structure can decrease the levelized cost of electricity (LCOE) (Baum et al., 2018) and
43 (Luengo and Kolios, 2015).

44 OWT support structures constantly experience cyclic stress imposed by wind turbulences and
45 wave loading which makes them prone to the fatigue failure (Barltrop and Adams, 1991). The
46 fatigue damage accumulation could be further accelerated if exposed to the corrosive marine
47 environment.

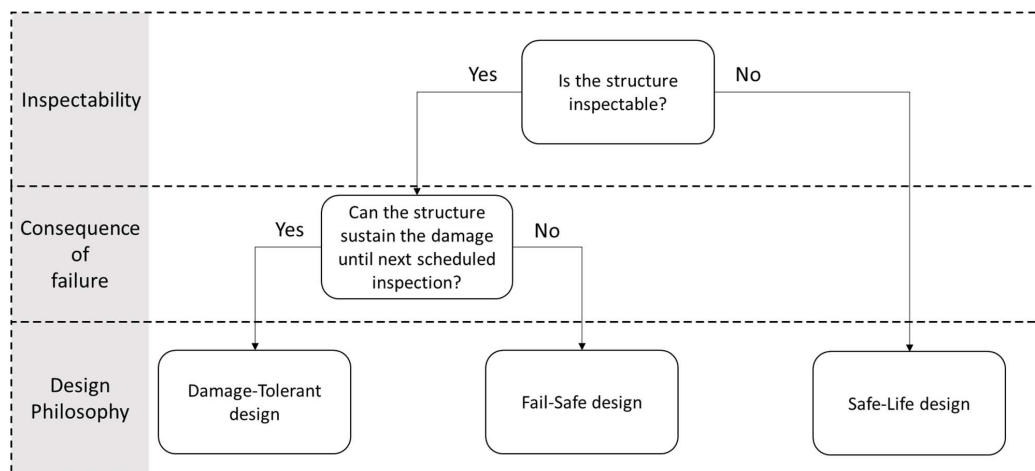
48 There are two approaches for quantifying fatigue damage: The S-N (Stress vs. Number of cycles)
49 method and the Fracture Mechanics (FM) approach.

50 Standards such as IEC 61400-3 (IEC, 2009), DNVGL-ST-0126 (DNVGL, 2016a), DNVGL-ST-
51 0437 (DNVGL, 2016b) and DNVGL-RP-C203 (DNV, 2010) are commonly used for the design of
52 offshore wind turbines against fatigue failure. Current design approaches are solely based on
53 the S-N method. In this approach fatigue life of a structural element is determined using a
54 relevant S-N curve, recommended by one of the standards or derived from bespoke fatigue test
55 programs. Service induced stresses, contributing to fatigue damage accumulations, are
56 determined from structural analysis then a suitable joint class capable of resisting those
57 stresses is specified. Alternatively, if the joint class is known, maximum allowable fatigue
58 stresses for the intended life of the structure is determined from the relevant S-N curve
59 (Hobbacher, 2008).

60 Fatigue design of steel structures using S-N data is commonly preferred to the Fracture
61 Mechanics approach due to its simplicity (Naess, 1985). The S-N approach is also considered
62 more reliable since it is based on fatigue test compared to the Fracture Mechanics which is
63 based on calculations where additional input variables (e.g. crack growth rate, toughness, and
64 residual stress distributions) need to be considered (Anderson, 2005).

65 Despite its popularity, a number limitations exist with the S-N data approach in relation to
66 offshore wind turbine structures:

67 **Design for inspection:** Many structures are designed considering a damage tolerant philosophy
68 where the structure is expected to tolerate certain levels of fatigue damage until next scheduled
69 inspection (Fig. 1). The expected crack size at the time of the inspection is estimated using
70 Fracture Mechanics and a suitable non-destructive testing (NDT) technique capable of detecting
71 the critical crack size is prescribed. The S-N approach can only quantify the accumulated
72 damage without providing any information about the size and dimensions of the damage.
73 Fracture mechanics on the other hand estimates time-dependent fatigue crack size. In OWT
74 structures, due to access restrictions, the choice of NDT method can be limited to a certain NDT
75 method with a specific detection capability. Therefore, it may be necessary to consider the
76 Probability of Non-Detection (POND) and improve the design for such a scenario.



77
78 **Figure 1 Relationship between inspection and fatigue design philosophy**

79 **Effect of larger defect sizes:** S-N data is based on the assumption that the initial defect sizes are
80 small, typically between 0.04 to 0.2 mm (BSI7608, 2015), assuming that an appropriate
81 fabrication quality control program is in place which can detect larger fabrication defects. In
82 practice, reliability and efficiency of such a program and the NDT techniques are uncertain and
83 vary considerably among fabrication yards (Amirafshari, 2019). Assessment and design of the
84 welded joints considering the presence of large defects is only possible using a Fracture
85 Mechanics approach. An improved joint design can be achieved allowing for possible fabrication
86 defects by, for example, specifying larger thicknesses, higher toughness steels, post weld heat
87 treatment, etc (Zerbst et al., 2015).

88 **New welding processes:** There are always efforts to improve structural resistance, fabrication
89 efficiency and weld quality by developing and implementing new welding technologies. Those
90 processes may inevitably have altered characteristics (defect rates, sizes, and geometry,
91 residual stresses, material toughness, etc.), which affect fatigue failure of the joint. Considering
92 these variables using S-N data will require development of bespoke fatigue test program which
93 is not always feasible (Lassen and Recho, 2013). A more efficient and cost-effective solution is
94 the application of fracture mechanics.

95 **New materials:** development and use of new steel grades with higher tensile strength and weld
96 consumable with superior weldability characteristics affects fatigue life. I.e. higher strength
97 steel will be capable of resisting higher stresses, but the fatigue resistance does not increase
98 proportionally (Okumoto et al., 2009). Contrary to the S-N method, these variables can be
99 directly considered in the fatigue life prediction using Fracture Mechanics.

100 **Shakedown, and compressive residual stresses:** Fracture failure of welded joints is directly
101 related to weld residual stresses. Tensile residual stress reduce fatigue life by reducing fracture
102 capacity and moving the compressive part of cyclic stress to the tensile stress region. Part of
103 these stresses can be relieved under service or fabrication loads, which is commonly known as
104 the “shake-down” effect (Li et al., 2007). In pile foundations, on the other hand, since the
105 structure is driven to the soil a considerable amount of compressive residual stresses are
106 induced into the pile (Da Costa et al., 2001), which can potentially improve the fatigue and
107 fracture performance. The effect of compressive residual stress and the shakedown phenomena
108 can be addressed using a fracture mechanics approach.

109 In this paper the fracture mechanics principals is briefly described, then a framework for an
110 optimised design of structures based on fracture mechanics is developed. Then, probabilistic



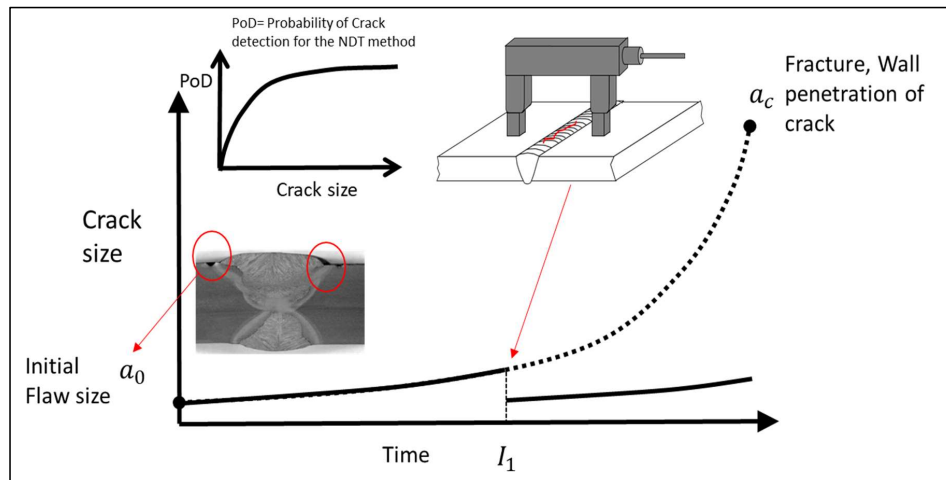
111 fracture mechanics for risk and reliability-based design approaches is outlined. Finally,
112 application of the developed methods to a Monopile support structure is demonstrated.

113 2 Fracture Mechanics Approach

114 Fatigue cracks in welded structures initiate from weld fabrication defects at the joints. Even
115 sound welded joints often contain small undercuts (Fig. 2).

116 Fracture mechanics approach uses the Paris equation to predict crack growth under cyclic
117 stress. The method is based on the assumption that an initial flaw is present at the structure.
118 The initial flaw size depends on the rigour of the fabrication quality control (QC) program
119 (Jonsson et al., 2013). The reliability of the NDT method that is used during the QC, the extent
120 of the inspection (100% or partial) and the flaw acceptance criteria will influence such a rigour.

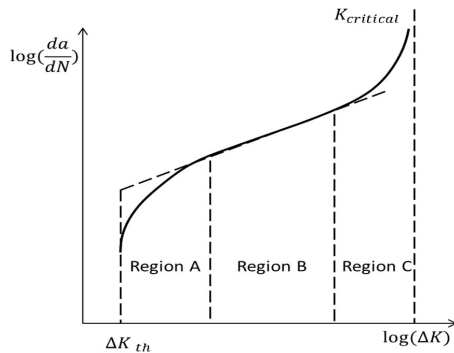
121 The fracture mechanics enables efficient application of NDT methods for in-service inspection
122 by specifying inspection interval(s) and the most effective NDT which has the capability of
123 reliable detection of the predicted crack size with a required confidence. This is illustrated in
124 Fig. 2 below, where the NDT inspection (I_1) detects cracks greater than initial flaw size (a_0). If
125 all such cracks are found and repaired the crack growth curve will be shifted down.



126
127 **Figure 2 Crack growth curve diagram**

128 2.1 Crack growth prediction

129 Fracture mechanics (FM) enables prediction of crack propagation by using the crack growth
130 rate, illustrated in Fig. 3. Region A is where crack growth rate occurs as soon as $\Delta K \geq \Delta K_{th}$,
131 where ΔK_{th} is the threshold value of ΔK . The threshold value depends on a number of factors
132 such as the stress ratio = K_{max}/K_{min} , sequence effect, residual stresses, loading frequency, and
133 the environment. Region B is where the crack growth rate increases with ΔK to a constant
134 power. Region C is where the crack growth rate increases rapidly until failure occurs as soon as
135 $K \geq K_{critical}$.



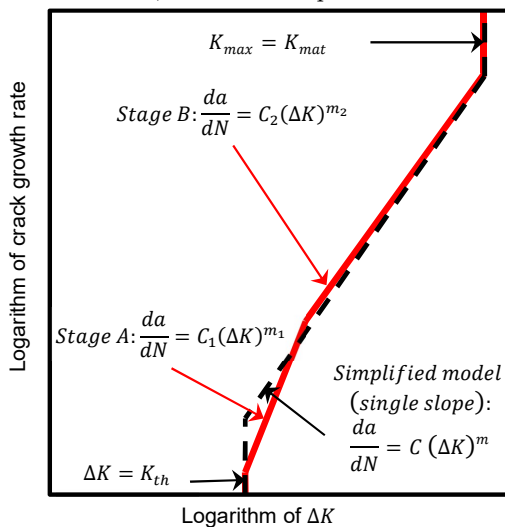
136

137 **Figure 3 Schematic of crack propagation curve according to Paris-Erdogan law (Amirafshari, 2019)**

138 In the FM approach crack growth rate is commonly described by the Paris-Erdogan Eq. (1):

$$\frac{da}{dN} = C * \Delta K^m \quad (1)$$

139 where, $\frac{da}{dN}$ is the rate of crack growth with respect to load cycles, ΔK is the change in stress
 140 intensity factor, and C and m are material constants. Recently a bilinear crack growth model
 141 has been used, as well (Fig. 4). BS7910:2015 (BS7910, 2015a) recommended model is the
 142 bilinear model, while the simplified model is cited, as well.



143

144 **Figure 4 Schematic of crack growth models by Paris law**

145 Stress intensity factor is described by:

$$\Delta K = Y\sigma\sqrt{\pi a} \quad (2)$$

146 where, a is flaw size, σ is stress at the flaw, and Y is the geometry function which depends on
 147 both the geometry under consideration and the loading mode. There are several ways in which
 148 solutions for Y can be obtained. Although it is possible to derive solutions for simple geometries



149 analytically, e.g. using ‘weight functions’, numerical techniques are more commonly used (finite
 150 elements, finite difference or boundary elements methods).

151 The number of cycles to failure is calculated by rearranging and nitrating Eq. (1):

$$N = \int_{a_0}^{a_f} \frac{da}{C(\Delta K)^m} = \frac{1}{A * Y^m * \Delta \sigma^m * \pi^{\frac{m}{2}}} * \frac{a_f^{(1-\frac{m}{2})} - a_0^{(1-\frac{m}{2})}}{1 - \frac{m}{2}} \quad (3)$$

152 Offshore structure are not subjected to constant amplitude stress, but a variable amplitude
 153 stress spectrum. If the long-term stress distribution is converted into a step function of n blocks
 154 generally of equal length in log N , the crack size increment for the step i is:

$$\Delta a_i = C(\Delta K_i)^m \Delta N_i \quad (5)$$

155 moreover, the final crack size at the end of the N cycles is obtained by summing Eq. (5) for the
 156 n stress blocks:

$$a_N = a_0 + \sum_{i=1}^N \Delta a_i \quad (6)$$

157 Equation (5) is only valid for small values of Δa_i since ΔK_i depends on the crack size, which
 158 requires dividing the stress range spectrum into a large number of stress blocks.

159 The number of cycles to failure may, alternatively, be calculated according to Eq. (7) using an
 160 equivalent constant amplitude stress ranges $\Delta \sigma_{eq}$ giving the same amount of damage (Naess,
 161 1985):

$$\Delta \sigma_{eq} = \left[\int_0^{\infty} \Delta \sigma^\beta p_{\Delta \sigma}(\Delta \sigma) d\Delta \sigma \right]^{1/\beta} \quad (7)$$

162 where β is the contribution factor. For the central part of the crack growth curve β is often taken
 163 as the slope of the of the crack growth line. $p_{\Delta \sigma}(\Delta \sigma)$ is the probability density function of stress
 164 range $\Delta \sigma$.

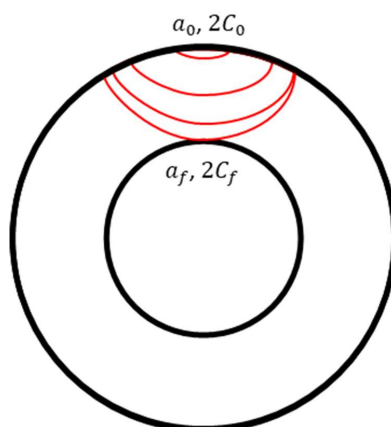
165 2.2 Failure criteria

166 2.2.1 Through thickness

167 In the through-thickness criterion, the initial fatigue crack is assumed to be a surface breaking
 168 flaw growing along the height (a) and length ($2C$) of the flaw. The failure happens when the
 169 crack height penetrates through the thickness of the wall (Fig. 5). This criterion is, particularly,



170 commonly adopted for structures containing pressurised containments e.g. pipe lines, pressure
171 vessels, etc.



172

173 **Figure 5 Diagram of a surface crack penetrating wall**

174 2.2.2 Total Collapse criteria

175 Many structures have the capacity to sustain through-thickness cracks until the crack length
176 reaches a critical length. Thin wide plates that are primarily subjected to membrane stress and
177 redundant structures such as jacket type platforms, and stiffened plate hull structures are
178 examples of such structures.

179 In structural reliability analysis the probability of a collapse can be considered as a probability
180 of a fatigue crack failure, P_F , times the probability of a collapse given that there is a fatigue
181 failure in the structure, P_{SYS} . The probability of the total structural collapse due to fatigue failure
182 should be below a target probability of failure, P_t :

$$P_F * P_{SYS} \leq P_t \quad (1)$$

183 For jacket structures the method of removing one member has been commonly used to assess
184 the residual capacity against overall collapse (DNV, 2015).

185 2.2.3 Critical crack size

186 The fatigue failure is considered to occur when the crack size reaches a critical value. There are
187 generally two ways to determine the critical size, which is explained in the coming sections:

- 188 1. Based on geometry of the structural member
- 189 2. Based on Failure Assessment diagram

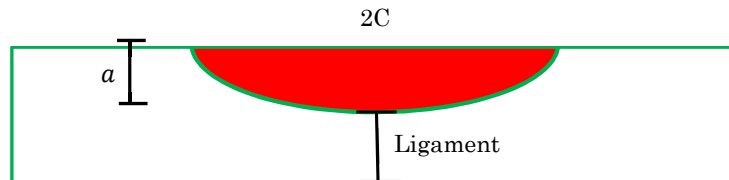
190 The critical size maybe then reduced to account for further safety factors.

191 2.2.3.1 Based on geometry of the structural member

192 For ductile structures, it is common to take the material thickness as the critical crack height
193 ($a_f = a_{cr} = \text{Thickness}$). However, normally the assumption is that the crack grows under cyclic
194 loading which corresponds to normal service loading until it becomes through thickness. In
195 reality, failure often happens during extreme load occurrences. The cracked structure may fail



196 under such extreme loading through failure of the thickness ligament (Fig. 6). The brittle or
197 elasto-plastic ligament failure may also occur in structures with low fracture toughness.



198

199 **Figure 6 Diagram of the remaining ligament in a semi-spherical crack**

200 To address above limitation the failure assessment diagram (FAD) may be adopted.

201 *2.2.3.2 Based on Failure Assessment Diagram (FAD)*

202 Failure Assessment Diagram (FAD) can assess the failure of the through-thickness crack as
203 well as implementing extreme load occurrences by treating them as the primary stress. The
204 approach is explained below.

205 When a crack propagates through a structure, ultimately the crack size reaches a critical size
206 a_f . a_f corresponds to a critical stress intensity factor, usually taken as characteristic of the
207 fracture toughness K_{mat} , at which fracture happens. Alternatively, if the applied load is high
208 and structure tensile strength is low, the structure may reach its tensile strength capacity and
209 fail by plastic collapse. The latter is more favourable as it is usually associated with large
210 deformations prior to failure providing some level of warning. In between brittle fracture and
211 global collapse is an elastoplastic failure mode, where failure occurs before reaching the plastic
212 capacity or toughness limit; this has been best described by failure assessment diagram (FAD)
213 in the R6 procedure in 1976 and improved over time by e.g. including the options available to
214 model specific material properties. The body of knowledge encapsulated in R6 affected the
215 development of British Standards documents in various ways over the years, leading to
216 BS7910:1999 and the latest version at the time of writing, (BS7910, 2015a).

217 The failure assessment line (FAL) represents the normalised crack driving force:

$$K_r = \frac{K_{elastic}}{K_{elastic\ plastic}} \quad (8)$$

218 K_r is equal to 1 where applied load is zero and declines as the ratio between applied load and
219 yield load (L_r) increases towards collapse load (see Fig. 6).

220 The plastic collapse load is calculated based on yield stress. However, the material has further
221 load carrying capacity as it work-hardens through yield to the ultimate tensile stress. To take
222 this into account the rightwards limit of the curve is fixed at the ratio of the flow stress to the
223 yield stress:

$$L_r = \frac{\sigma_{flow}}{\sigma_Y} \quad (9)$$

224 The flow stress is the average of the yield and ultimate stresses:



$$\sigma_{flow} = \frac{\sigma_Y + \sigma_U}{2} \quad (10)$$

225 If the assessment point lies inside the envelope (below the FAL), the fracture mechanics driving
 226 parameter is lower than the materials resistance parameter and the part should be safe,
 227 otherwise there is a risk of failure. The failure assessment diagram can be determined with one
 228 of the procedures provided by (BS7910, 2015a). As it is illustrated in Fig. 6, FAD may be
 229 categorised into three different zones: Zone 1 is the fracture dominant zone, Zone 2 is the
 230 elastoplastic region or the knee region, and Zone three is the collapse dominant zone.

231 (BS7910, 2015a) has three alternative approaches Option 1, Option 2 and Option 3. These are
 232 of increasing complexity in terms of the required material and stress analysis data but provide
 233 results of increasing accuracy.

234 Option 1 (BS7910, 2015a) is a conservative procedure that is relatively simple to employ and
 235 does not require detailed stress/strain data for the materials being analysed. The Failure
 236 Assessment Line (FAL) for the Option 1 analysis is given by:

$$K_r = f(L_r) = (1 + 0.5 * L_r^2)^{-0.5} * (0.3 + 0.7 * \exp(-\mu * L_r^6)) \quad (11)$$

237 for $L_r < 1$, where: $\mu = \min\left[0.001 \frac{E}{\sigma_Y}; 0.6\right]$.

238 and:

$$K_r = f(L_r) = f(1)L_r^{(N-1)/2N} \quad (12)$$

239 For, $1 < L_r < L_{r,max}$, where N is the estimate of strain hardening exponent given by: $N = 0.3(1 -$
 240 $\frac{\sigma_Y}{\sigma_{UTS}})$. and $L_{r,max} = \frac{\sigma_{flow}}{\sigma_Y}$.

241 Option 2A/3A of BS 7910:2005 generalised FAD, is similar but not identical to Option 1 (BS7910,
 242 2015a)

$$K_r = (1 - 0.14 * L_r^2) * (0.3 + 0.7 * \exp(-0.65 * L_r^6)) \quad (13)$$

243 The BS7910:2015 Option 2 FAD is based on the use of a material-specific stress-strain curve.
 244 The assessment line can be written as:

$$K_r = f(L_r) = \left[\frac{E \varepsilon_{ref}}{L_r \sigma_Y}, \frac{L_r^3 \sigma_Y}{2E \varepsilon_{ref}} \right]^{-0.5} \quad (14)$$

245 ε_{ref} is the true strain obtained from the uniaxial tensile stress-strain curve at a true stress
 246 $L_r \sigma_Y$.

247 The option 3 failure assessment curve is specific to a particular material, geometry and loading
 248 type using both elastic and elastic-plastic analyses of the flawed structure It is given by:

$$f(L_r) = \sqrt{\frac{I_e}{J}}, \text{ for } L_r < L_{max} \quad (15)$$

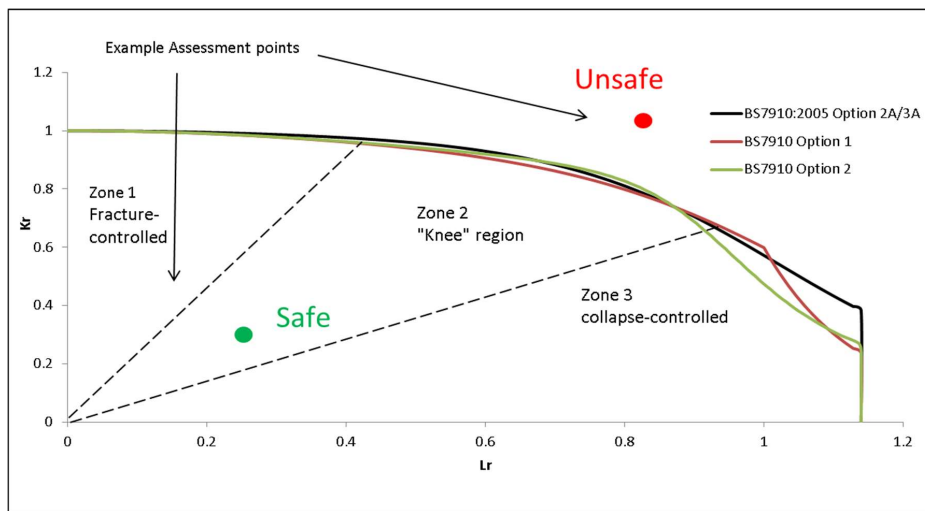
249



$$f(L_r) = 0, \text{ for } L_r > L_{max} \quad (16)$$

250 J_e is the value from the J-integral from the elastic analysis at the load corresponding to the
251 value L_r . The Option 3 curve is not suitable for general use. It is useful only for specific cases as
252 an alternative approach to Options 1 and 2 (BS7910, 2015a).

253 Options 1&2 (BS7910, 2015a) and Option 2A/3A (BS7910, 2015a) for structural steel with
254 tensile stress of 550 MPa and Yield stress of 450 MPa are illustrated in Fig. 6. It can be seen
255 that the greatest difference between the three plotted locus is in the collapse region.



256
257 **Figure 7 Failure Assessment Diagram (FAD)** (Amirafshari, 2019)

258 3 Fracture Mechanics framework for structural design

259 The common practice in structural design is to specify dimensions of the structural component
260 based on the most critical limit state, usually ultimate limit state (ULS), and check or modify
261 the design based on other limit states such as serviceability limit state (SLS) or fatigue limit
262 state (FLS).

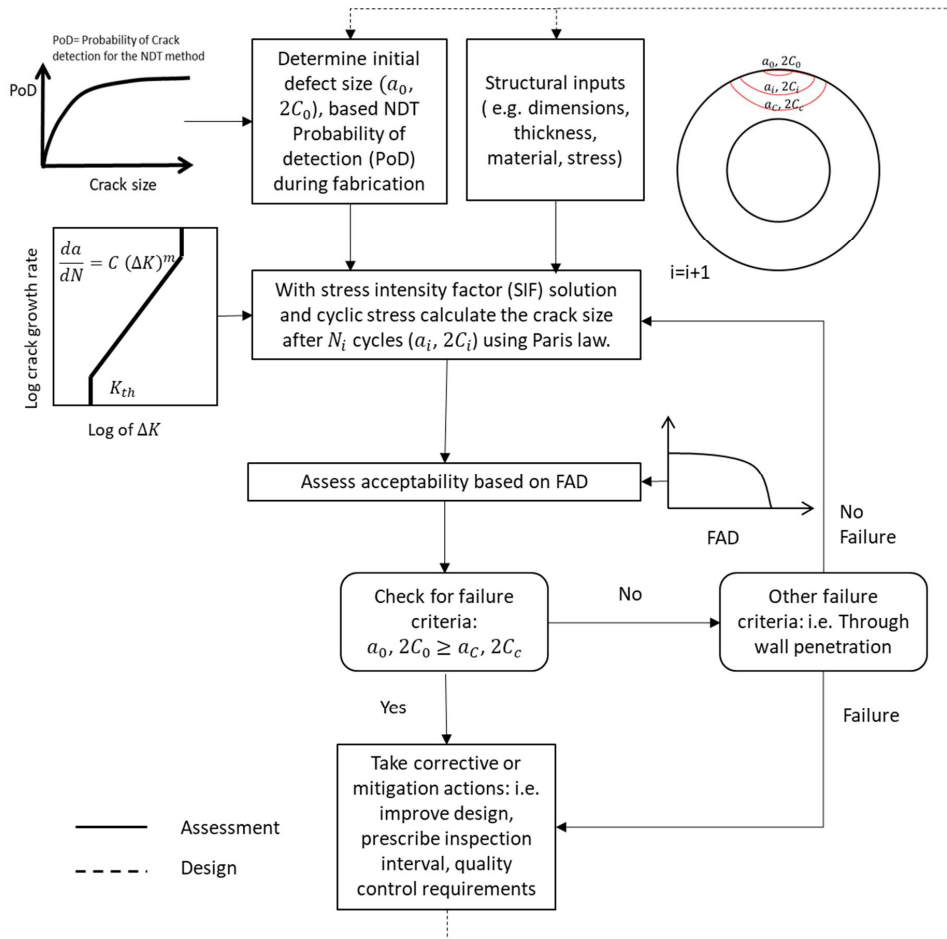
263 In OWT support structures fatigue failure initiates from the welded connection, thus, the
264 fatigue design often involves prescribing local improvements to the welded connection. However,
265 since fatigue life is related to dynamic characteristics of the structure the global dimensions of
266 the structure may also need alterations to achieve higher fatigue resistance.

267 The fatigue damage prediction model could be the S-N curve method or the Linear Elastic
268 Fracture Mechanics (LEFM). Here, a LEFM method is adopted to address the limitations of the
269 S-N curve method. Fig. 7 shows the proposed framework.

270 First, the required inputs, such as structural dimensions (determined by structural design
271 based on ULS), initial flaw size, material toughness and tensile properties, stress at the flaw,
272 and parameters of Paris equation, are determined, the using the Paris equation for a chosen
273 increment of time (N_i), the increase in initial crack size is estimated. The predicted crack size is
274 then compared against failure criteria. The procedure is repeated for the next time increment
275 until the failure. If the failure is predicted to occur before intended life of the structure the



276 fatigue life may be enhanced by changing variables that affect the fatigue failure such as
 277 structural dimensions, quality control requirements (initial flaw size), post fabrication
 278 improvements (e.g. post weld heat treatment), or by specifying inspection interval(s).

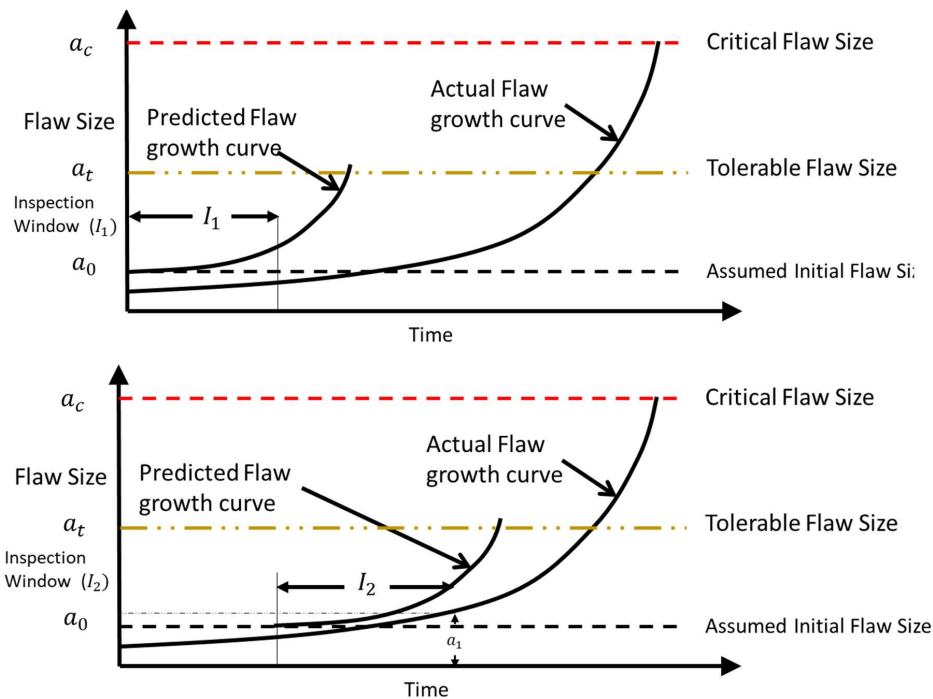


279
 280 **Figure 8 Fracture Mechanics flow diagram for assessment and design of structures against fatigue failure**

281 3.1 Damage-tolerant design

282 The term damage-tolerance fracture mechanics normally refers to a design methodology in
 283 which fracture mechanics analyses predict remaining life, and specifies inspection intervals.
 284 This approach is typically applied to structures prone to time dependent crack growth. The
 285 damage tolerance philosophy allows flaws to remain in the structure, provided they are well
 286 below the critical size.

287 Once the critical crack size has been estimated, a safety factor is applied to determine the
 288 tolerable flaw size a_t . The safety factor should be based on uncertainties in the input parameters
 289 (e.g. stress, parameters in the Paris equation and toughness). Another consideration in
 290 specifying the tolerable flaw size is the crack growth rate; a_t should be chosen such that da/dt
 291 at this flaw size is relatively small, and a reasonable length of time is required to grow the flaw
 292 from a_t to a_c (Anderson, 2005). This is shown schematically in Fig. 8.

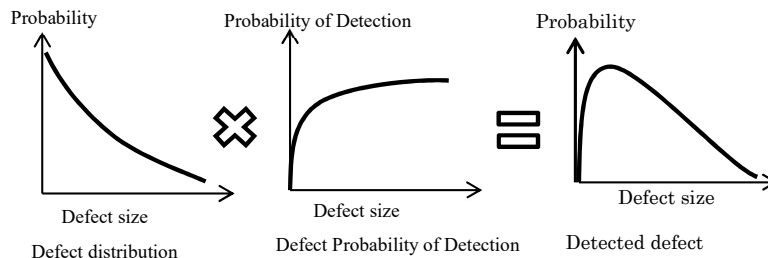


293

294 **Figure 9** schematic representation of damage tolerant fracture mechanics approach, adapted from (Anderson, 2005)

295 **3.2 Inspection reliability (PODs)**

296 NDT techniques can only detect a limited number of defects of a certain size. For instance, an
 297 NDT method with 50% probability of detection at a certain size, is expected to miss 50% of the
 298 defects of that size, in other words, the real number of the defects with that size is likely to be
 299 100% more than the detected. In structural integrity assessment, it is often convenient to plot
 300 detection probability against defect size, which constructs the so-called probability of detection
 301 curve (Fig. 10). Detection capabilities of NDT methods are directly related to the sizing of flaws
 302 (Georgiou, 2006). The bigger the flaw sizes, the more likely that they are detected. Fig. 9 shows
 303 the relationship between detected defect size distribution, the probability of detection of defect
 304 sizes and the actual defect size distribution that are present in the structure.



305

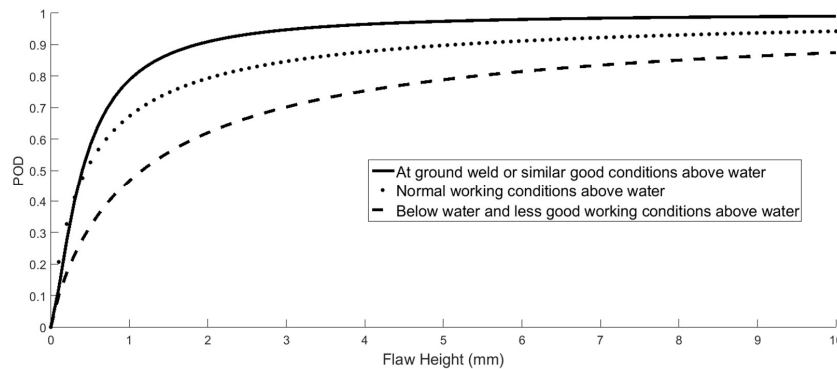
306 **Figure 10** Relationship between crack size distribution, Probability of detection and detected crack size distribution
 307 (Amirafshari, 2019)

308 PoDs for NDT methods are highly dependent on various factors such as, the operator skills,
 309 testing environment, test specimen (thickness, geometry, material, etc.), type of the flaw,
 310 orientation and location of the flaw (Førli, 1999). Hence, accurate estimation of PoD curves



311 requires individual PoD test programs for specific projects. However, a number of lower bound
 312 generic models are available in the literature for some specific NDT methods. Two of such
 313 models, that are relevant to this work, are given in Fig. 10 and Table 1 below.

314 Further information about derivation, application and limitations of PoD can found in
 315 (Georgiou, 2006).



316
 317 **Figure 11 DNV POD for surface NDE. Replotted from (DNV, 2015)**

Method	Condition	Flaw Length mm	Flaw through-thickness mm	
Magnetic Particle Inspection (MPI)	Machined or ground	5	1.5	
	As-welded	With local dressing	10	2
		With poor profile	20	4
Ultrasonic Testing (UT)	Convictional	15	3	

318 **Table 1 NDT Reliability (BS7910, 2015b)**

319 3.3 Inspection strategy

320 Fracture mechanics assessment is closely tied to inspection method. The inspection method
 321 provides input to the fracture mechanics assessment, which in turn helps to define inspection
 322 intervals. A structure is inspected during construction for quality control purposes. Choice of
 323 the NDT method varies between fabrication yards, but as a general rule all weldments are
 324 visually inspected and may be complemented by inspection of limited number of checkpoints
 325 using more reliable NDT techniques on a sampling basis (Amirafshari et al., 2018). If no
 326 significant flaws are detected, the initial flaw size is set at an assumed value a_0 , which
 327 corresponds to the largest flaw that might be missed by NDE.

328 Generally, there are two strategies in inspection of structures that are susceptible to damage
 329 mechanisms:

330 3.3.1 The inspection schedules are fixed (Periodic Maintenance):

331 Here, the fracture mechanics can be used to design the structure so that the possible fatigue
 332 cracks remain below tolerable limits. The crack size at the time of inspection is predicted using
 333 the Paris law in order to select an appropriate NDT method.

334 3.3.2 Inspection schedule is not fixed (Condition Based Maintenance):

335 In this case, the inspection interval and the NDT method can be optimised in such a way that
 336 the inspection results in a safer condition or a minimised cost of maintenance and failure.



337 **3.4 Design inputs**

338 Design inputs can be categorised into design constraint (Table 2) and design variables (Table 3).
 339 Here, only design variables related to a fracture mechanics method are considered. Further
 340 information about design of offshore wind turbine support structures can be found in (Arany et
 341 al., 2017) and (Van Wingerde et al., 2006).

342 Depending on chosen maintenance strategy the inspection capabilities may be considered as
 343 design constraint or design variable.

344 If a probabilistic approach is employed instead of the conventional deterministic approach, the
 345 variables are considered stochastically and target probabilities of failures are used instead of
 346 allowable deterministic values (Table 2).

Design Constraint		
Limit State	Deterministic	Allowable damage, stress, etc.
	Probabilistic	Target levels of reliability
Inspection capabilities	During fabrication	<ul style="list-style-type: none"> • Extend of inspection • NDT PoD
	During service	<ul style="list-style-type: none"> • Inspection schedule (fixed periodic inspections) • NDT method (e.g. POD, access restrictions, costs)

347 **Table 2 Design constraints for damage tolerant fracture mechanics design**

Design variables	Inspection and Monitoring options (Condition Based Maintenance)	NDT methods Condition monitoring
	Design options	Structural design options: <ul style="list-style-type: none"> • Thickness • Redundancy • Material selection Fabrication specifications: <ul style="list-style-type: none"> • Weld profile improvements • Post Weld Heat Treatment • Quality Control (i.e. NDT during fabrication, Tolerance limits)

348 **Table 3 Design variables for damage tolerant fracture mechanics design**

349 **4 Probabilistic Fracture Mechanics**

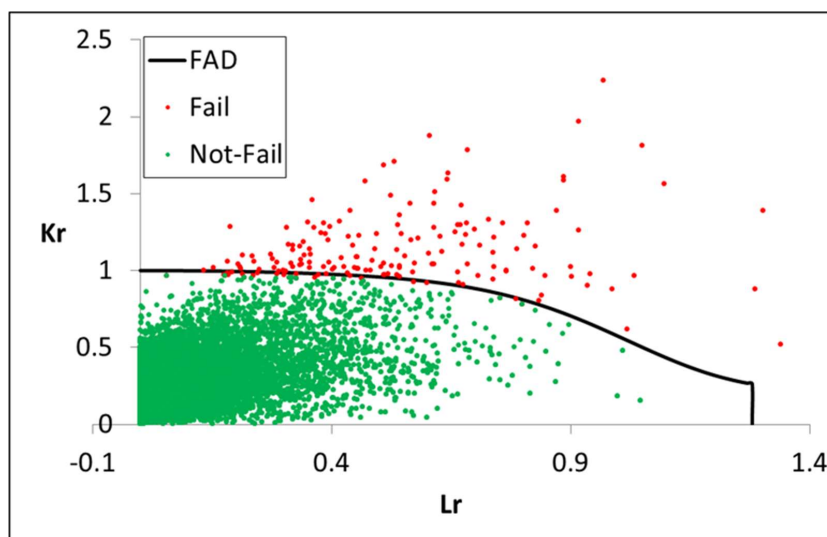
350 Fracture mechanics approaches are commonly used deterministically and generally have a
 351 hierarchical nature, i.e. the analyst may progressively reduce the level of conservatism in
 352 assumptions by increasing the complexity level of the analysis and consequently the precision
 353 of results until the operation of the structure is found to be fit-for-service. Otherwise, the
 354 structure will require a repair, a reduction of service (for example lowering primary stress) or
 355 resistance improvements (i.e. reduction of secondary stresses by stress relief techniques). This
 356 type of approach is particularly useful in the assessment of safety cases where the aim is to
 357 demonstrate that the structure is safe.

358 In deterministic analyses, uncertainty in variables are dealt with by taking upper bound and
 359 lower bound of those variables- upper bound values of applied variables such as stress and flaw
 360 size, with lower bound values of resistance variables such as fracture toughness. In reality, the
 361 probability of all unfavourable conditions occurring at the same time is very low and often too



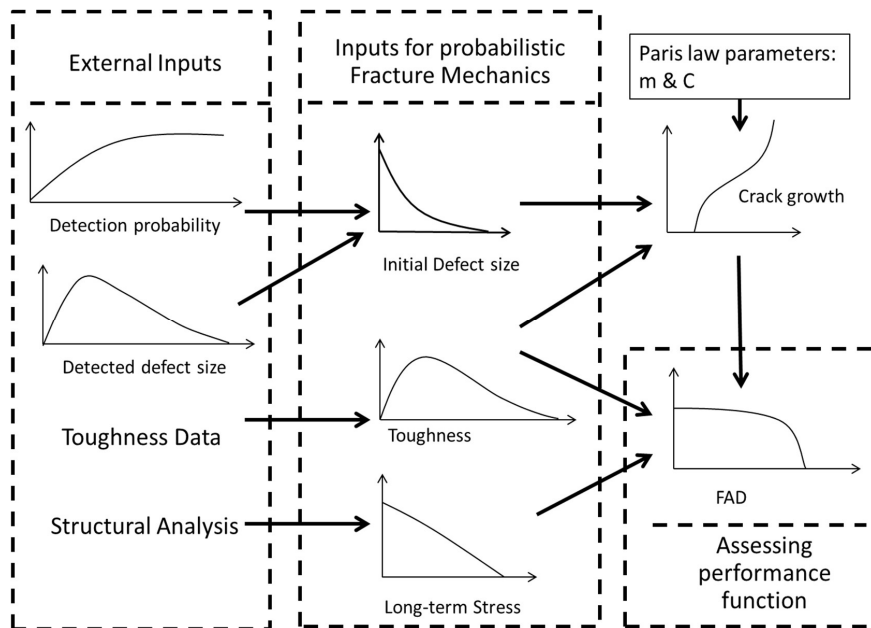
362 conservative. An alternative approach is a probabilistic analysis, in which, uncertain variables
363 are treated stochastically and as random variables.

364 In probabilistic assessments, all possible combinations of input variables leading to failure are
365 compared against total possible combinations, and a probability of failure is estimated instead
366 of a definite fail or not-fail evaluation. Probabilistic analysis is also in-line with the damage
367 tolerant philosophy. The failure probability for the limit state function may be estimated using
368 one of available analytical, numerical or simulation methods such Monte Carlo simulation.
369 Figure 12 shows Probabilistic fracture assessment using Monte Carlo method and based on the
370 FAD.



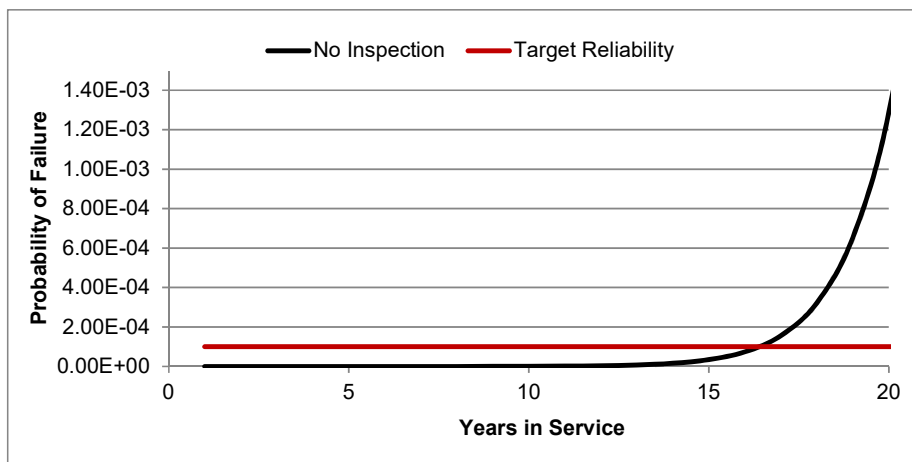
371
372 **Figure 12 Probabilistic fracture assessment using Monte Carlo method and based on FAD (Amirafshari, 2019)**

373 One limitation of deterministic fracture mechanics is that conservative prediction of critical
374 defect size and the time to the failure may reduce inspection efficiency by targeting wrong defect
375 sizes and at a wrong time in service, whereas probabilistic assessment will provide a more
376 efficient result (Lotsberg et al., 2016). Probabilistic failure assessment of the structures is also
377 known as Reliability analysis. These two terminologies are often used interchangeably.



378
 379 Figure 13 A schematic presentation of the inputs to Probabilistic Fracture Mechanics (Amirafshari, 2019)

380 Figure 18 shows schematic presentation of the inputs to probabilistic fracture mechanics.
 381 Probabilistic fatigue and fracture analysis will predict the time-dependent failure probability of
 382 the structure (Fig. 19). The predicted reliability will then need to be compared against an
 383 appropriate target reliability level.



384
 385 Figure 14 Example of a time-dependent fatigue and fracture reliability curve

386 4.1 Target reliability levels

387 Target reliability values may be employed to ensure that a required level of safety is achieved.
 388 The target reliability measures depend on the failure consequence as well as the cost and effort
 389 to reduce the risk of failure. The consequence of failure can be the risk of human injury and
 390 fatality, economic consequence, and social impacts. The target reliability should always
 391 correspond to a reference period, e.g. annual or service life probability of failure. If the relevant



392 consequence is the risk of human life, annual failure probabilities are preferred to ensure a
 393 consistent level of tolerable risks at any time. Target reliabilities maybe defined in four different
 394 ways:

- 395 1. The standard developers recommend a reasonable value. This method is used for novel
 396 structures.
- 397 2. Reliability implied by standards. The level of risk is estimated for a design standard that is
 398 considered to be satisfactory. This method has been commonly used for standard revisions,
 399 particularly where the intention has been to provide a more uniform safety level for different
 400 structural types and loading types. By carrying out a reliability analysis of the structure
 401 satisfying a specific code using a given probabilistic model, the implicit required level in this
 402 code will be obtained, which may be applied as the target reliability level. The advantage
 403 with this approach compared to applying a predefined reliability level is that the same
 404 probabilistic approach is applied in the definition of the inherent reliability of the code
 405 specified structure and the considered structure, reducing the influence of the applied
 406 uncertainty modelling in the determination of the target reliability level.
- 407 3. The target level for risk assessment based on failure experiences. This method is particularly
 408 useful when the functional reliability of the system is more important than the reliability of
 409 individual components. In the automotive industry or electronic components manufacturing
 410 component reliability is determined by failure rate data of real components. The failure rate
 411 data is then used in system reliability calculation(Bertsche, 2008).
- 412 4. Economic value analysis (cost-benefit analysis). Target reliabilities are chosen to minimise
 413 total expected costs over the service life of the structure. In theory, this would be the
 414 preferred method, but it is often impractical because of the data requirements for the model.
 415 Examples of target reliabilities prescribed by codes and standards are listed in Table 6. For
 416 further information about available models for developing target reliability levels for novel
 417 structures reference is made to (Bhattacharya et al., 2001).

	Scope	Limit state function	Minimum Reliability index	Maximum Probability of failure
Euro code. Basis of structural design (BSI, 2005)	buildings and civil engineering works	Ultimate limit states (ULS)	3.3 to 4.3 for 50 years reference period and 4.2 to 5.2 for annual	4.83×10^{-4} to 8.54×10^{-6} for 50 years reference period and 1.33×10^{-5} to 9.96×10^{-8} for annual
	Residential and office buildings, public buildings where consequences of failure are medium (e.g. an office building)	Fatigue limit state (FLS)	1.5 to 3.8 for 50 years reference period	6.68×10^{-2} to 7.23×10^{-5} for 50 years reference period
DNV (DNV, 1992)	Marine structures		3.09 to 4.75	1.00×10^{-3} to 1.02×10^{-6}



IEC61400-1	Offshore Wind Turbines	ULS & FLS	3.3	5.00 x 10 ⁻⁴
DNV_OS_J101	Offshore Wind Turbines (unmanned structures)	ULS		1.00 x 10 ⁻⁴
DNV_OS_J101	Offshore Wind Turbines (manned structures)	ULS		1.00 x 10 ⁻⁵

418 **Table 7** Examples of target levels of reliabilities specified by standards

419 **4.2 Risk Based design**

420 The purpose of risk analysis is to comprehend the nature of risk and its characteristics
 421 including, where appropriate, the level of risk. Risk analysis involves a detailed consideration
 422 of uncertainties, risk sources, consequences, likelihood, events, scenarios, controls and their
 423 effectiveness. An event can have multiple causes and consequences and can affect multiple
 424 objectives (ISO-31000, 2018). Risk remaining after protective measures are taken is called
 425 residual risk (ISO-14971, 2012). The purpose of risk evaluation is to support decisions. Risk
 426 evaluation involves comparing the results of the risk analysis with the established risk criteria
 427 to determine where additional action is required (ISO-31000, 2018). The overall procedure for
 428 risk analysis and risk evaluation is a risk assessment (ISO-31000, 2018).

429 A commonly used method of risk evaluation is the so-called Risk Matrix model in which the
 430 failure probability is shown in one axis and the consequence of failure on the other. The
 431 failure probability and consequence failure maybe specified quantitatively, qualitatively, or
 432 semi-quantitatively, depending on the complexity of the model and the availability of data. Each
 433 combination of failure probability and consequence of failure will then be assigned a
 434 corresponding risk level. It is useful to show these levels in specific colour coding convention.
 435 One such convention is an adapted traffic light convention in which low-risk levels are shown
 436 in green, extreme risks in red and medium risk levels are coloured in yellow. It is also possible
 437 to refine this colour coding further, for example, light yellow and dark yellow, to allow for more
 438 risk levels. An example Risk Matrix is shown in Fig. 22.

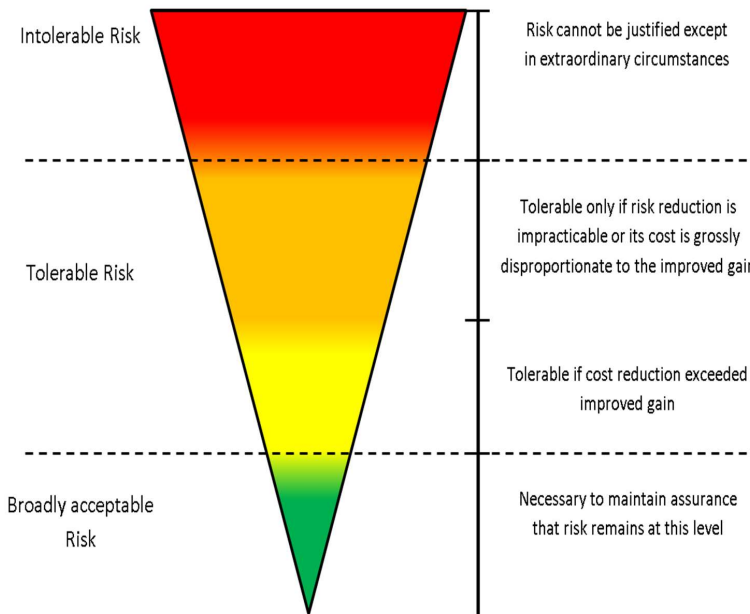
Probability of failure	5. Frequent	HIGH	HIGH	EXTREME	EXTREME	EXTREME
	4. Likely	MEDIUM	HIGH	HIGH	EXTREME	EXTREME
	3. Possible	MEDIUM	MEDIUM	HIGH	HIGH	EXTREME
	2. Unlikely	LOW	MEDIUM	MEDIUM	HIGH	HIGH
	1. Rare	LOW	LOW	MEDIUM	HIGH	HIGH
		1. Negligible	2. Minor	3. Moderate	4. Major	5. Catastrophic
Consequence of failure						

439 **Figure 15** A typical Risk matrix diagram

440 In order to assign an appropriate risk level (i.e. colour in the risk matrix) it is necessary to
 441 establish risk acceptance levels. If a system has a risk value above the accepted levels, actions
 442 should be taken to improve the safety through risk reduction measures. One challenge in this
 443 practice is defining acceptable safety levels for activities, industries, structures, etc. Since the
 444 acceptance of risk depends upon society perceptions, the acceptance criteria do not depend on
 445 the risk value alone (Ayyub et al., 2002).

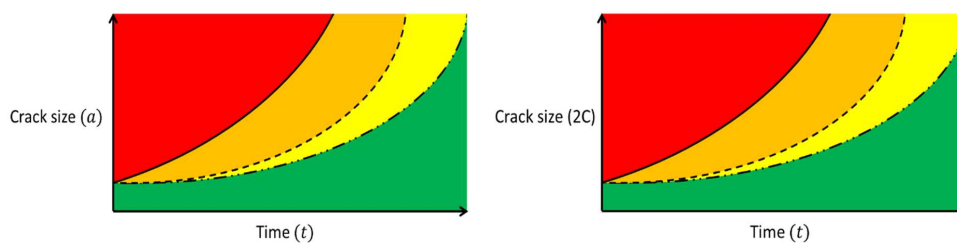


446 Another common risk evaluation method is the ALARP, which stands for "as low as reasonably
447 practicable", or ALARA (as low as reasonably achievable) (HSE, 2001). The ALARP basis is that
448 tolerable residual risk is reduced as far as reasonably practicable. For a risk to be ALARP, the
449 cost in reducing the risk further would be grossly disproportionate to the benefit gained. The
450 basis of ALARP is illustrated by the so-called carrot diagram in Fig. 23.



451
452 **Figure 16 ALARP Carrot diagram based on (HSE, 2001)**

453 By adopting a risk based approach in fracture mechanics for a chosen design parameter the
454 structural design may be assessed against the corresponding risk. As an example, the design
455 stress levels for a particular initial crack size will be associated with the corresponding risk
456 levels, as schematised in Fig. 24.



457
458 **Figure 17 schematics of Crack growth curves based risk profile**

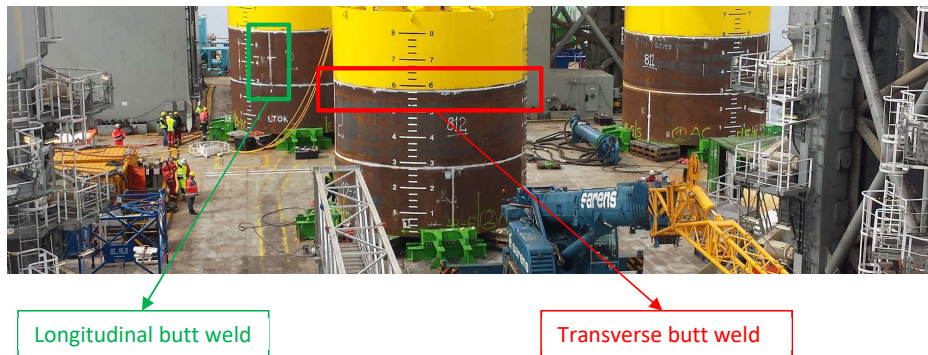
459 5 Case-Study 1: Monopile OWT support structure

460 Fatigue design based of a baseline NREL 5MW offshore wind turbine (OWT) supported on a
461 monopile structure (Fig. 12) is presented here. The framework illustrated in Fig. 7 is used to
462 conduct the fracture mechanics assessment. Table 5 summarises inputs parameters used in this
463 study. Further information about the structure and the Finite Element Analysis can be found
464 in (Gentils et al., 2017).



465 Transverse butt weld (weld line perpendicular to the normal stress) are more prone to fatigue
 466 damage than the longitudinal butt joints (weld line parallel to the normal stress). Figure 9
 467 shows these joints in a monopile structure. A fatigue crack growing at the transverse butt weld
 468 toe located in mud-line (Fig. 12) is considered as the most critical location.

469

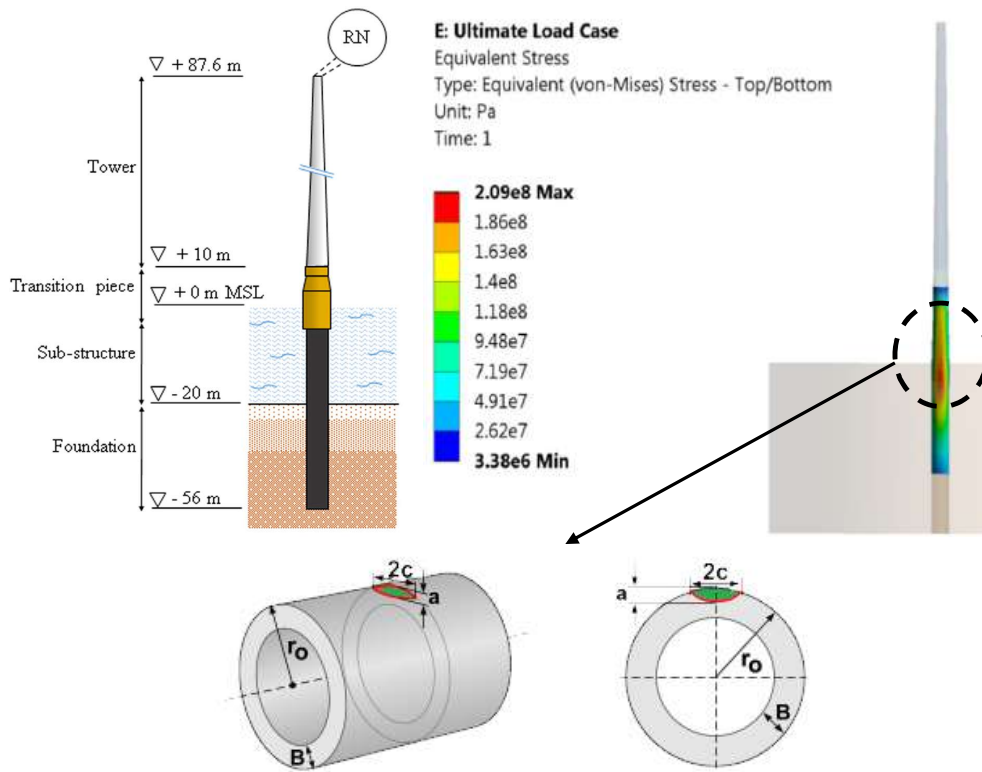


470

471 Figure 18 Monopile welded connections (twd, 2019)

Case Description		
Structure	NREL 5MW OWT	
Material Properties	Young Modulus	210
	Poisson Ratio	0.38
	Yield stress	355
	Tensile strength	550
	Toughness	200 MPa* m ^{0.5} assumed
Fatigue assumptions	Crack growth model	Single slope Crack growth
	Cyclic stress	Equivalent constant amplitude stress 51.2 MPa
	Stress Intensity Solution	Surface flaw in a Plate
	Paris Law Constants	$m = 3.9, C = 3.814 * 10^{-16}$ for Crack growing in HAZ and in Air, $m = 3.3, C = 4.387 * 10^{-14}$ for Crack in HAZ and in with free corrosion, (for da/dN in mm/cycle, and ΔK , in $N/mm^{0.5}$), (Mehmanparast et al., 2017)
	Design cycles in life	$N_{life} = \eta_a * \eta_{rated} * (20 [year] * 365 [day per year] * [hour per year] * 60 [min per hour])$, for this structure = $1.253 * 10^8$ (Gentils et al., 2017)
Fracture assumptions	FAD	BS 7910 Option 1
	Primary stress	209 MPa
	Secondary stress	Weld Residual stress= 100 MPa, assumed
	Thickness (B)	60 (mm)
	Initial Flaw dimensions (a*2C)	(1.5 mm * 5 mm)

472 Table 5 Inputs for Fatigue and fracture mechanics assessment



473

474 **Figure 19** The case study structure diagrams and FEA contour plots for the support structure

475 Fatigue cracks normally initiate from small toe undercut weld defects (Fig. 2), thus, in this
 476 study a semi-spherical flaw growing in heat affected zone (HAZ) of the joint is considered. NDT
 477 inspection techniques are used during fabrication as part of quality control scheme. MPI and
 478 UT are effective, and commonly used method to detect surface breaking and embedded flaws,
 479 respectively. Here, initial flaw size is conservatively assumed to be equal to 90 % PoD the NDT
 480 methods (Table 1). Primary fracture stress is taken as caused by ultimate limit state (ULS)
 481 design stress (Fig. 12) corresponding to the parked wind turbine, under the 50-years Extreme
 482 Wind Model (EWM) with the 50-years Reduced Wave Height (RWH) and Extreme Current
 483 Model (ECM), defined as the Design Load Case (DLC) 6.1b and 2.1 for (IEC, 2019) and (DNV,
 484 2013) standards, respectively. The crack growth stress is taken as the fatigue load case
 485 corresponds to an operating state under Normal Turbulence Model (NTM) and Normal Sea
 486 State (NSS) where wave height and cross zero periods are obtained from the joint probability
 487 function of the site, assuming no current; it corresponds to the DLC 1.2 from the IEC standard
 488 (IEC, 2019) and is assumed to represent the entire fatigue state (Gentils et al., 2017). Paris law
 489 parameters reported by (Mehmanparast et al., 2017) for offshore wind monopile weldments has
 490 been adopted. Other key assumptions and inputs for fatigue and fracture mechanics assessment
 491 are given in Table 5.

492 5.1 Crack growth in Air

493 Crack growth parameters in Paris equation for ferritic steels depend on the, cyclic stress ratio,
 494 and environmental condition (Amirafshari and Stacey, 2019). In presence of effective corrosion
 495 protection measures, in-air conditions apply (BS7910, 2015a).

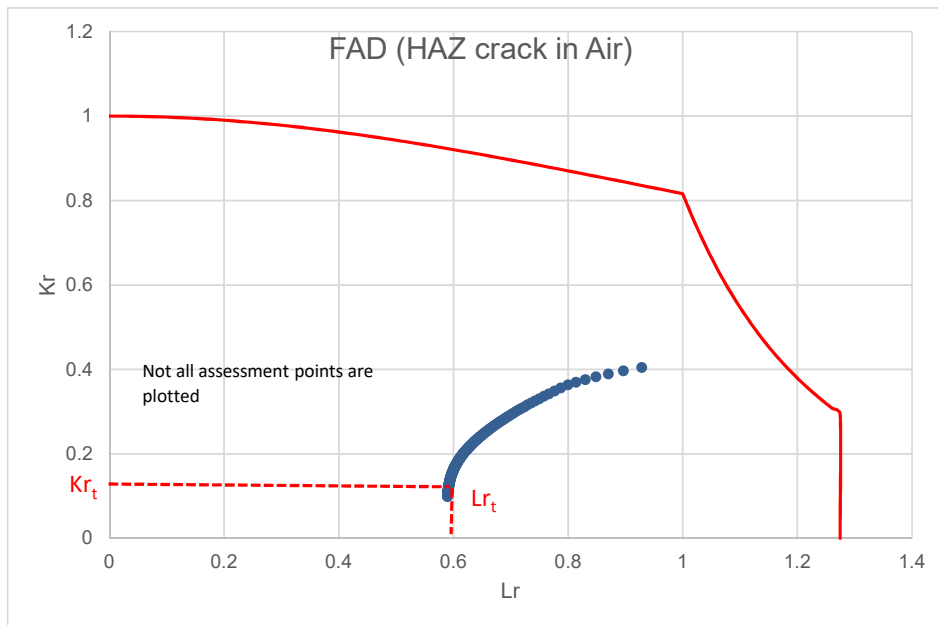


496 Fatigue and fracture assessment results for cracks propagation in air environment are given in
 497 Table 5. In a tolerant design, the tolerable crack sizes need to be selected way below critical
 498 sizes by considering some level of safety factors (Anderson, 2005). As described earlier, the
 499 chosen tolerable crack size needs to be determined in a region of crack size where crack growth
 500 rate with respect to time is small to allow for a long time before failure but large enough to be
 501 detected by the in-service inspection technique. Here, tolerable crack height of 5.2 mm is chosen
 502 which, depending on the inspection condition (Fig. 10), gives 70 to 90 percent Probability of
 503 Detection (PoD). As shown in Fig. 20, this will provide a good margin of safety and at least 6
 504 years before failure (Fig. 22).

Assessment results		
Critical Crack size	$a_c = 45 \text{ mm}$	$2C_c = 116 \text{ mm}$
Tolerable crack size (Assumed)	$a_t = 5.2 \text{ mm}$	$2C_t = 12 \text{ mm}$
	$Lr_t=0.592$	$Kr_t=0.128$

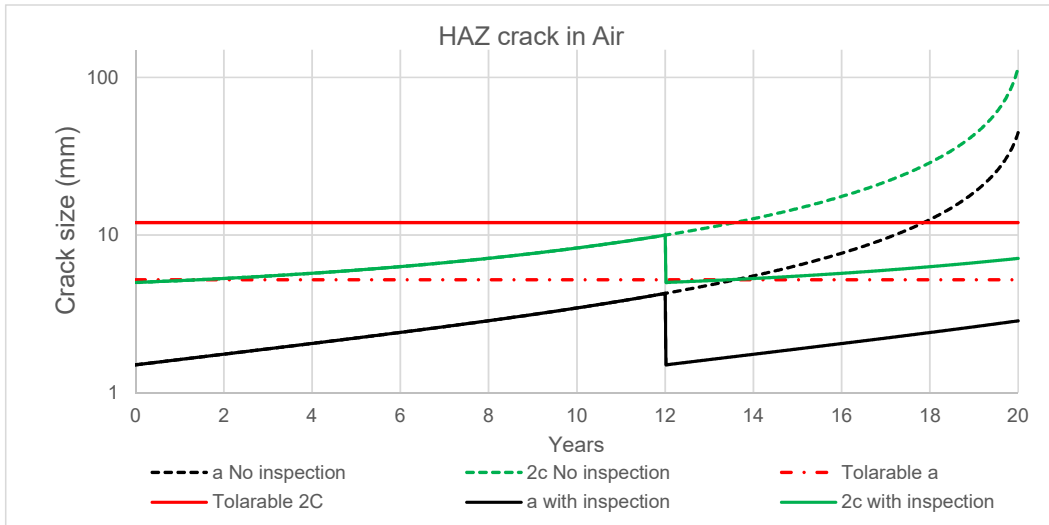
505 Table 6 results for crack growth in HAZ and in Air environment

506 Figure 20 shows assessment points from initial crack propagation at start of service life to the
 507 final year of service. If the service continues beyond the design life (20 years), the structure is
 508 likely to fail in elasto-plastic mode, providing reasonable level of plasticity from safety point of
 509 view.



510
 511 Figure 20 Failure assessment diagram (FAD) for crack growth in HAZ and in Air environment without inspection

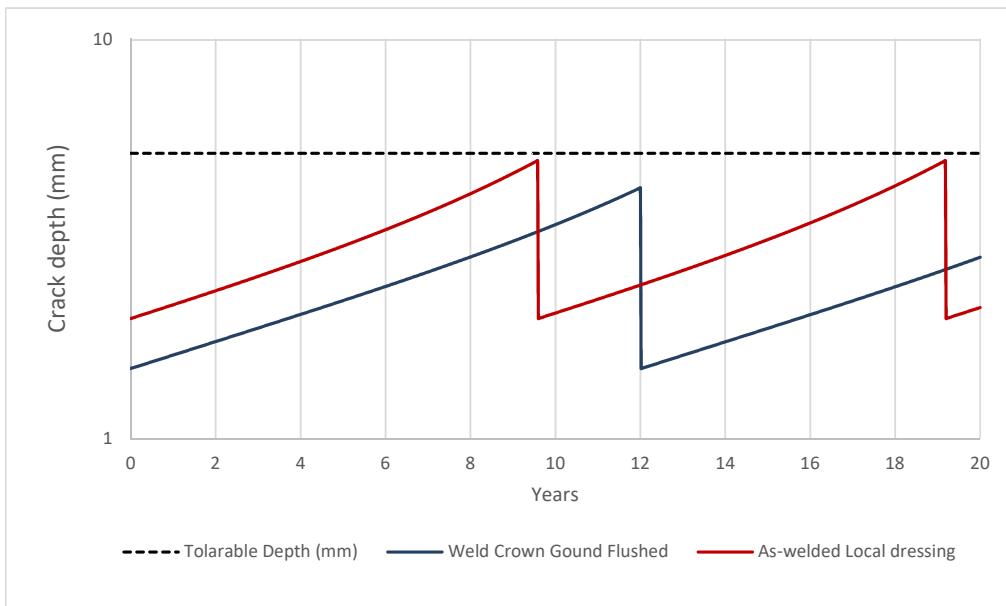
512 As explained earlier a damaged tolerant design is closely tied to in-service inspection. Here, it
 513 is assumed that a MPI inspection is carried out at year 12. When no crack is detected or repaired
 514 if detected, the predicted crack size is updated and reduced back to the initial crack size. This
 515 is shown with solid lines after year 12 in Fig. 14. The final year crack size remains below the
 516 tolerable limits.



517

518 **Figure 21 Crack growth curves for propagation in HAZ and in Air environment**

519 The weld profile condition may be as- welded or ground flushed depending on fabrication
 520 specification and could be altered by the design engineer. The effect of such condition was
 521 studied by considering the influence of weld profile on POD for the MPI method. MPI can find
 522 smaller cracks in the welds with ground flushed crowns (Table 1). As shown in Fig. 21 improving
 523 the weld joint design by specifying ground flushing requirement reduces the inspection
 524 frequency from twice to once in 20 years of service.



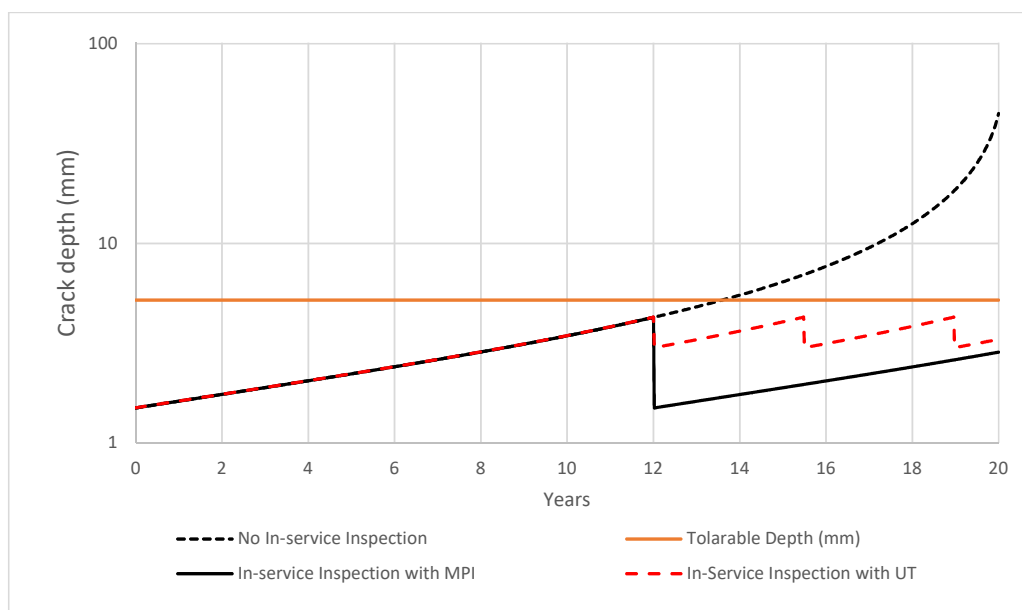
525

526 **Figure 22 Effect of weld profile condition on in-service inspection**

527



528 The effect of choice NDT for in-service inspection was studied by considering a case where UT is
529 chosen as the inspection method. The detection reliability specified in Table 1 used to determine
530 the crack size that can be left undetected after inspection. Figure 22 shows the predicted crack
531 size compared to inspection with MPI. It is observed that in order to keep the crack size below
532 tolerable size three inspections are required instead of one inspection using MPI.

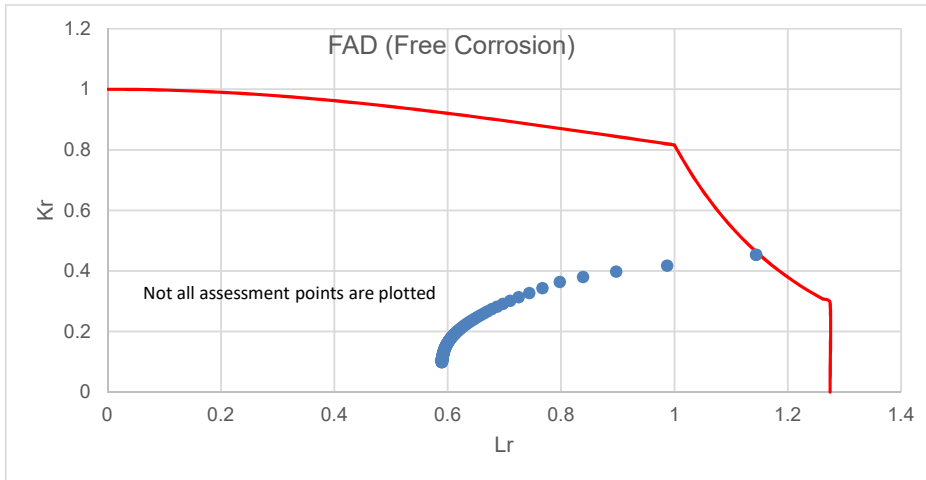


533

534 **Figure 23 Selection of NDT method based on probability of detection and crack size at the time of inspection**

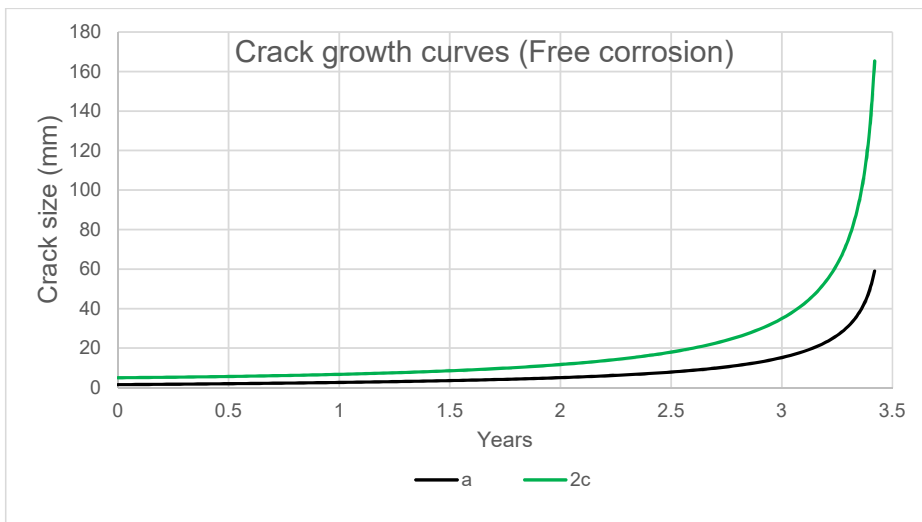
535 5.2 Effect of environment

536 In the event of insufficient corrosion protection, the fatigue crack growth will be accelerated.
537 The accelerated crack growth rate is reflected in fracture mechanics through changing the Paris
538 law constants to those observed in corrosive environment. This is shown in Fig. 15 and Fig. 16,
539 where the previously studied defect is assessed under free corrosion environment instead of the
540 air environment. It is observed that failure is predicted to occur as early as 3.4 years after
541 commissioning. One strategy could be an increased attention to execution of corrosion protection
542 measures prior to commissioning. Additionally the joint should be inspected for the signs of
543 corrosion at least every three years.



544
545

Figure 24 Failure assessment diagram (FAD) for crack growth in HAZ and with free corrosion



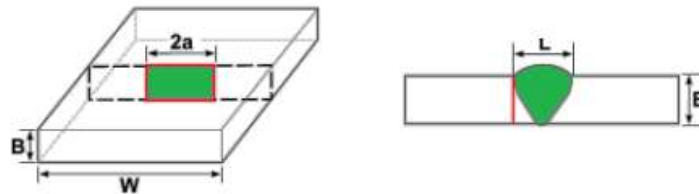
546

547 Figure 25 Crack growth curves for propagation in HAZ and with free corrosion

548 6 Case-Study 2: Probabilistic Fracture Mechanics application to 549 a plate failure

550 Many structure members in offshore can tolerate cracks even after they become through
551 thickness. These structures may be idealised by plates containing through thickness cracks (Fig.
552 20). This can be for example for a less critical location of the structure in case-study 1 with lower
553 stress levels.

554 Here, application of probabilistic fracture mechanics to such a structure is demonstrated. The
555 assumed inputs are listed in Table 7.



556
 557 **Figure 26 Through-thickness Crack geometry diagram**

Case Description		
Case study structure	Offshore topside Platform with Long-term stress shape parameter = 0.85 and load cycle rate = 5.063 cycles/ min	
	Maximum design stress = 0.62 * Yield stress	
Material Properties	Young Modulus	210 constant
	Poisson Ratio	0.3 constant
	Yield stress (Y_S)	450 constant
	Tensile strength	560 constant
	Toughness	200 MPa* m ^{0.5} assumed
Fatigue assumptions	Crack growth model	Single slope Crack growth
	Cyclic stress	Equivalent constant amplitude stress 21 MPa
	Stress Intensity Solution	Through-thickness flaw in an infinite Plate
	Paris Law parameters	BS 7910 recommended values
	Design cycles in life	$N_{life} = load\ cycle\ rate\ (\frac{cycles}{min}) * (20\ [year] * 365\ [day\ per\ year] * [hour\ per\ year] * 60\ [min\ per\ hour])$, for this structure = $5.322 * 10^7$
Fracture assumptions	FAD	BS 7910 Option 1
	Primary stress	Weibull distribution with scale parameter 9.47 MPa
	Secondary stress	Weld Residual stress= Constant 100 MPa, assumed
	Thickness (B)	60 (mm)
Inspection Capabilities	Initial Flaw dimensions (2a)	Exponential distribution with mean value of 2 mm
	In-service surface inspection	Surface inspection for ground welds above water surface (Fig. 10)

558 **Table 8 Inputs for probabilistic Fatigue and fracture mechanics assessment**

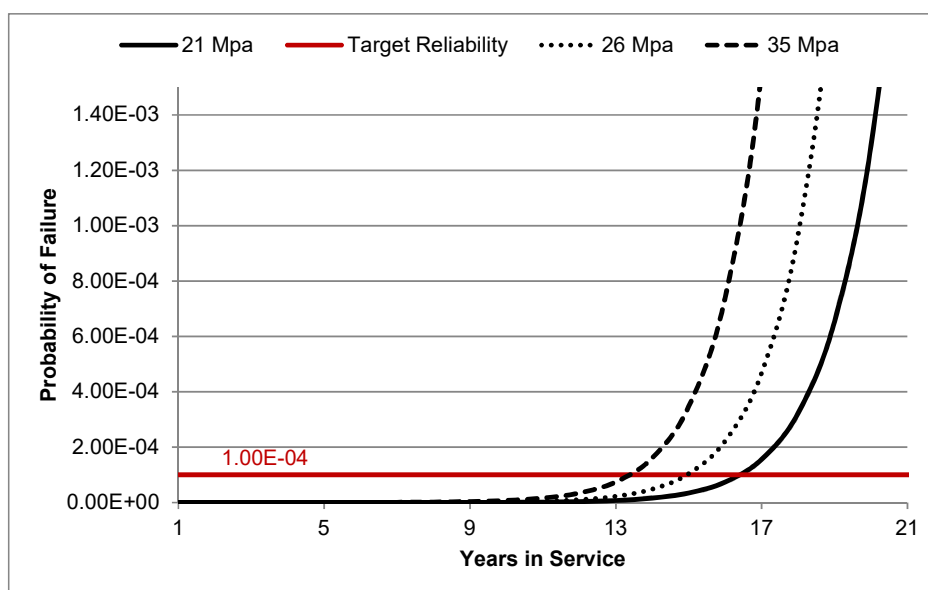
559 Figure 21 shows fatigue and fracture reliability of the structure under three levels of equivalent
 560 constant amplitude cyclic stress. As a starting point, 21 MPa cyclic stress which corresponds to
 561 extreme stress of $0.62 Y_S$ is selected. Target reliability level of 1.00×10^{-4} from Table 6 for
 562 Offshore Wind Turbines (unmanned structures) is selected. The structure will reach to the
 563 target tolerable probability of failure just before year 17, suggesting that the structure should
 564 be inspected prior this time. As it is shown in Fig. 25, such an inspection will reduce the failure
 565 probability below the target level for the rest of the intended service life.

566 If the aim was to design the structure to the safe-life design philosophy, the stress would have
 567 needed to be reduced below current level. This, however, may not be an economical option since
 568 the current extreme stress level already possesses significant safety factor ($0.62 Y_S$) and



569 reducing the stress will require bigger cross sectional dimensions and, hence, a heavier and
570 more expensive structure. Integrating in-service inspection options in design can potentially
571 result in a more efficient design.

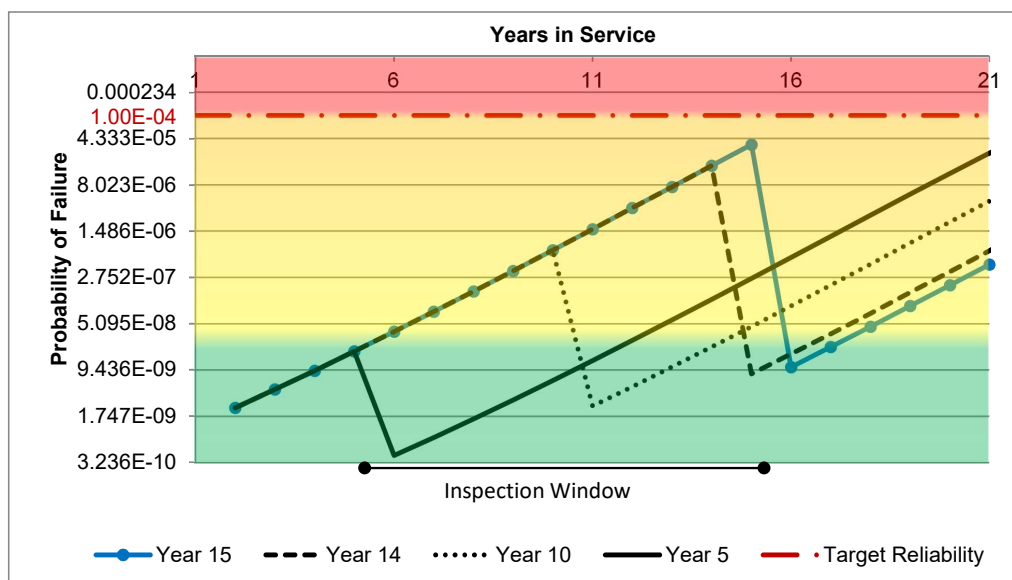
572 Furthermore, the design cyclic stress may be increased considering the availability of in-service
573 inspection. Two stress levels are considered here: An upper bound limit value of 35 MPa
574 corresponding to extreme stress equal to the Yield stress and a moderate value of 26 MPa. As
575 depicted in Fig. 21, the probability of failure curve will be shifted to left 2 and 3 years,
576 respectively. It is evident that the structure can sustain higher levels of stresses provided that
577 appropriate time for inspection is determined and also other required limit states are not
578 violated.



579
580 **Figure 27 Fatigue reliability (FM) of a welded joint in an offshore structure for three different constant amplitude**
581 **stresses**

582 The effect of an inspection schedule is considered for the case of through-thickness crack under
583 21 MPa cyclic stress. It was shown previously in Fig. 21 that, the structure is predicted to reach
584 the target tolerable probability of failure just before year 17, thus, the inspection should be
585 scheduled prior to this time. Here, a number of inspection options are considered.

586 Any inspection earlier than year 6 appears to have little benefit as the failure probabilities are
587 below $5.0E-8$, a very low probability of failure. The reduction in probability of failure is in the
588 order of one and the structure is likely to exceed the target level of reliability again close to the
589 final year of service. Inspection between year 10 to 15 show the most effective results by keeping
590 the structure way below the target level throughout and to the end of service life ensuring
591 considerable level of safety as well as providing further life extension possibilities in the final
592 years of designed service life.



593
594

Figure 28 Crack growth curves of case study through thickness in a plate considering different first inspection times

595 7 Conclusions

596 This paper presented a new approach in fatigue design of offshore wind turbine support
597 structures. Traditionally, design of offshore renewable structures against fatigue failure has
598 been performed using the so-called S-N curve method. This approach, however, suffers from a
599 number of limitations, such as limited ability to integrate the inspection capabilities. The
600 structural design can significantly benefit from inspectability of the structure by considering
601 the damage-tolerant nature of many offshore structures. Fracture mechanics is a powerful tool
602 capable of address a wide range limitations associated with of the S-N approach.

603 In this work, a framework for design of offshore structures based on fracture mechanics was
604 developed and its applications to a monopile wind turbine support structure were demonstrated.
605 Additionally, probabilistic fracture mechanics approach and its application in optimising in-
606 service NDT inspection for a plated structure under see wave loading was presented.

607 It was found that the design of the structure can be enhanced through specifying weld crown
608 improvements which leads to better fatigue performance and reduced in-service inspection. The
609 Magnetic Particle Inspection (MPI) will require three times less inspection interval than
610 Ultrasonic Testing (UT).

611 The probabilistic model showed to have the capability to account for uncertainty in design and
612 inspection variables including NDT reliability. It also provides a likelihood of failure which can
613 be used to calculate the risk associated with the chosen inspection time and in turn for
614 optimising inspection using a, for example, cost benefit analysis.

615 Additionally, the proposed optimisation model can be used for any practice of structural
616 optimisation of OWT support structures



617 Authors contribution

618 PA conducted the research, created the proposed framework, performed all case study analysis,
619 made the figures, and planned and wrote the paper. BF and AK contributed to the research with
620 intensive discussions and added to the paper with conceptual discussions and internal review.
621 AK secured the funding for this paper.

622 Competing of interest

623 The authors declare that they have no conflict of interest.

624 Acknowledgments

625 This work was supported by a grant from the Supergen Wind Hub EP/L014106/1, from the UK
626 Engineering and Physical Sciences Research Council (EPSRC), under the Flexible Funding
627 Scheme for University Strathclyde. Furthermore, this project has received funding from the
628 European Union's Horizon 2020 research and innovation program under grant agreement No.
629 745625 (ROMEO, 2019).

630 References

- 631 Amirafshari, P.: Optimising Non-destructive Examination of newbuilding ship hull structures
632 by developing a data-centric risk and reliability framework based on fracture mechanics,
633 University of Strathclyde., 2019.
- 634 Amirafshari, P. and Stacey, A.: REVIEW OF AVAILABLE PROBABILISTIC MODELS OF
635 THE CRACK GROWTH PARAMETERS IN THE PARIS EQUATION, in OMAE2019-961,
636 OMAE., 2019.
- 637 Amirafshari, P., Barltrop, N., Bharadwaj, U., Wright, M. and Oterkus, S.: A Review of
638 Nondestructive Examination Methods for New-building Ships Undergoing Classification
639 Society Survey, *J. Sh. Prod. Des.*, 33(2), 1–11, 2018.
- 640 Anderson, T. L.: *Fracture Mechanics: Fundamentals and Applications*, 2005.
- 641 Arany, L., Bhattacharya, S., Macdonald, J. and Hogan, S. J.: Design of monopiles for offshore
642 wind turbines in 10 steps, *Soil Dyn. Earthq. Eng.*, 92, 126–152,
643 doi:10.1016/j.soildyn.2016.09.024, 2017.
- 644 Ayyub, B. M., Akpan, U. O., Rushton, P. A., Koko, T. S., Ross, J. and Lua, J.: Risk-informed
645 inspection of marine vessels., 2002.
- 646 Barltrop, N. D. P. and Adams, A. J.: *Dynamics of fixed marine structures*, Butterworth-
647 Heinemann., 1991.
- 648 Baum, S., Von Kalben, C., Maas, A. and Stadler, I.: Analysis and Modelling of the Future
649 Electricity Price Development by taking the Levelized Cost of Electricity and large Battery
650 Storages into Account, 2018 7th Int. Energy Sustain. Conf. IESC 2018, 1–8,
651 doi:10.1109/IESC.2018.8440005, 2018.
- 652 Bertsche, B.: *Reliability in automotive and mechanical engineering: determination of*
653 *component and system reliability*, Springer Science & Business Media., 2008.
- 654 Bhattacharya, B., Basu, R. and Ma, K.: Developing target reliability for novel structures: the
655 case of the Mobile Offshore Base, *Mar. Struct.*, 14(1–2), 37–58, 2001.
- 656 BS7910, B. S.: BS 7910:2013+A1:2015, Br. Stand. Institutions, London, 2015, 2015a.



- 657 BS7910, B. S.: BS 7910:2013+A1:2015 AnnexJ, 2015b.
- 658 BSI: BS EN 1990: 2002+ A1: 2005--Basis of Structural Design, 2005.
- 659 BSI7608: Guide to fatigue design and assessment of steel products, London BSI Stand. Publ.,
660 2015.
- 661 Da Costa, L. M., Danziger, B. R. and Lopes, F. D. R.: Prediction of residual driving stresses in
662 piles, *Can. Geotech. J.*, 38(2), 410–421, doi:10.1139/cgj-38-2-410, 2001.
- 663 DNV: Structural reliability analysis of marine structures, Det Norske Veritas., 1992.
- 664 DNV: Fatigue design of offshore steel structures, No. DNV-RP-C203, 2010.
- 665 DNV: Design of offshore wind turbine structures, DET NOR SKE Verit., 2013.
- 666 DNV: DNVGL-RP-C210-Probabilistic methods for planning of inspection for fatigue cracks in
667 offshore structures, 2015.
- 668 DNVGL: DNVGL-ST-0126: Support Structures for Wind Turbines, Oslo, Norw. DNV, 2016a.
- 669 DNVGL: DNVGL-ST-0437 Loads and site conditions for wind turbines., 2016b.
- 670 European Environment Agency: Share of EU energy consumption from renewable sources,
671 2005–2050., 2019.
- 672 Førli, O.: Guidelines for Development of NDE Acceptance Criteria, Nordtest., 1999.
- 673 Fraile, D., Komusanac, I. and Walsh, C.: Wind energy in Europe: Outlook to 2023., 2019.
- 674 Gentils, T., Wang, L. and Kolios, A.: Integrated structural optimisation of offshore wind
675 turbine support structures based on finite element analysis and genetic algorithm, *Appl.*
676 *Energy*, 199, 187–204, 2017.
- 677 Georgiou, G. A.: Probability of Detection (POD) curves: derivation, applications and
678 limitations, *Jacobi Consult. Ltd. Heal. Saf. Exec. Res. Rep.*, 454, 2006.
- 679 Hobbacher, A.: RECOMMENDATIONS FOR FATIGUE DESIGN OF WELDED JOINTS AND
680 COMPONENTS, 2008.
- 681 HSE: HSE's decision-making process, edited by HSE, HSE., 2001.
- 682 IEC: 61400-3 (2009) Wind Turbines—Part 3: Design Requirements for Offshore Wind
683 Turbines, 2009.
- 684 IEC: BS EN IEC 61400-1: Wind turbines part 1: Design requirements, *Int. Electrotech.*
685 *Comm.*, 2019.
- 686 ISO-14971: BS EN ISO 14971: 2012—Application of risk management to medical devices,
687 2012.
- 688 ISO-31000, B. S.: 31000,(2018) Risk management--Principles and guidelines, *Int. Organ.*
689 *Stand. Geneva, Switz.*, 2018.
- 690 Jonsson, B., Dobmann, G., Hobbacher, A., Kassner, M. and Marquis, G.: IIW guidelines on
691 weld quality in relationship to fatigue strength, *IIW Doc.*, 13, 2510–2513, 2013.
- 692 Lassen, T. and Recho, N.: Fatigue life analyses of welded structures: flaws, *John Wiley &*
693 *Sons.*, 2013.



- 694 Li, L., Moan, T. and Zhang, B.: Residual stress shakedown in typical weld joints and its effect
695 on fatigue of FPSOs, in ASME 2007 26th International Conference on Offshore Mechanics and
696 Arctic Engineering, pp. 193–201., 2007.
- 697 Lotsberg, I., Sigurdsson, G., Fjeldstad, A. and Moan, T.: Probabilistic methods for planning of
698 inspection for fatigue cracks in offshore structures, *Mar. Struct.*, 46, 167–192, 2016.
- 699 Luengo, M. M. and Kolios, A.: Failure mode identification and end of life scenarios of offshore
700 wind turbines: A review, *Energies*, 8(8), 8339–8354, doi:10.3390/en8088339, 2015.
- 701 Mehmanparast, A., Brennan, F. and Tavares, I.: Fatigue crack growth rates for offshore wind
702 monopile weldments in air and seawater: SLIC inter-laboratory test results, *Mater. Des.*, 114,
703 494–504, 2017.
- 704 Naess, A.: *Fatigue handbook: offshore steel structures*, 1985.
- 705 Okumoto, Y., Takeda, Y., Mano, M. and Okada, T.: *Design of ship hull structures: a practical
706 guide for engineers*, Springer Science & Business Media., 2009.
- 707 ROMEO: ROMEO, [online] Available from: <https://www.romeoproject.eu/>, 2019.
- 708 twd: Monopile Fabrication, [online] Available from: [https://twd.nl/suction-bucket-jacket-
709 seafastening-structures/suctionbucketjacket_seafastening_clamps_overview/](https://twd.nl/suction-bucket-jacket-seafastening-structures/suctionbucketjacket_seafastening_clamps_overview/), 2019.
- 710 Van Wingerde, A. M., Van Delft, D. R. V., Packer, J. A. and Janssen, L. G. J.: *Survey of
711 support structures for offshore wind turbines.*, 2006.
- 712 Zerbst, U., Klingner, C. and Clegg, R.: Fracture mechanics as a tool in failure analysis—
713 Prospects and limitations, *Eng. Fail. Anal.*, 55, 376–410, 2015.
- 714